pSPICA Force Field Extended for Proteins and Peptides

Yusuke Miyazaki and Wataru Shinoda*

Research Institute for Interdisciplinary Science, Okayama University, 3-1-1 Tsushima-naka, Kita-ku, Okayama 700-8530, Japan

E-mail: shinoda@okayama-u.ac.jp

Abstract

Many coarse-grained (CG) molecular dynamics (MD) studies have been performed to investigate biological processes involving proteins and lipids. Since CG force fields (FFs) in these MD studies often use implicit or non-polar water models to reduce computational costs. CG-MD using water models cannot properly describe electrostatic screening effects owing to the hydration of ionic segments, and thus cannot appropriately describe molecular events involving water channels and pores through lipid membranes. To overcome this issue, we developed a protein model in the pSPICA FF, in which a polar CG water model showing the proper dielectric response was adopted. The developed CG model greatly improved the transfer free energy profiles of charged side chain (SC) analogues across the lipid membrane. Application studies on melittin-induced membrane pores and mechanosensitive channels in lipid membranes demonstrated that CG-MDs using the pSPICA FF correctly reproduced the structure and stability of the pores and channels. Furthermore, the adsorption behavior of the highly charged nona-arginine peptides on lipid membranes changed with salt concentration, indicating the pSPICA FF is also useful for simulating protein adsorption on membrane surfaces.

1 Introduction

Molecular dynamics (MD) simulations have become a well-established method for providing deep insight into phenomena in biological systems at the molecular level. MD simulations have been used to reveal the structure, dynamics, and thermodynamic properties of various biological molecules such as lipids and proteins. With significant improvement in computer performance and the development of computational algorithms, MD simulations that allow the calculation of such properties are now relatively easy to achieve using all-atom (AA) force fields (FFs).[1] However, biological processes, especially those involving multiple proteins, essentially require microsecond and tens-of-nanometer scales; therefore, even with the powerful hardware and software currently available, most of these processes are still beyond the capabilities of AA-MD simulations.

Coarse-grained (CG) MD simulations are alternative approaches used to address molecular-level events that occur over longer time and larger spatial scales.[2] Many CG models and coarse-graining schemes have been proposed and developed to simulate biological phenomena involving lipids and proteins.[3–10] SPICA is the one such quantitative CG model that enables highly accurate simulations of biological and soft material systems.[11] It was originally developed to precisely predict morphological changes in self-assembled structures formed by surfactants and lipids,[12–16] and has recently been extended to simulate peptides and proteins.[17–19] In the CG parameterization scheme of the SPICA protein model, the following properties were well reproduced: experimental solvation free energies of protein side chain (SC) analogues, dimerization free energies of several transmembrane peptides, radial distribution functions (RDFs) between SC analogue dimers, and transfer free energy of SC analogues across lipid membranes obtained from AA simulations using CHARMM36,[20] the penetration depths and tilt angles of peptides on lipid membranes obtained from the Orientations of Proteins in Membranes (OPM) database. Owing to the SPICA parameterization scheme, which combines the top-down and bottom-up approaches, the developed protein model reproduces several thermodynamic properties and reasonably predicts the structure of protein

aggregates. However, because SPICA employs an explicit CG water model represented by a single uncharged Lennard-Jones (LJ) particle, it is difficult to capture molecular processes, particularly those involving the water pores formed by proteins in lipid membranes.

pSPICA is an alternative CG model based on a polar water model and was developed for the simulation of lipid membranes.[21] Except for the differences in the polarity of the water model and treatment of electrostatic interactions, pSPICA is almost identical to SPICA, and the interaction parameter optimization procedure in pSPICA follows that in SPICA. Therefore, pSPICA can reproduce several experimental thermodynamic properties and distribution functions of the AA-MDs. Thanks to the polar CG water model, CG-MD simulations with pSPICA successfully predicted the free energy barriers required for lipid flip-flop with water defects comparable to AA results, changes in the morphology of charged lipid aggregates with salt concentration, and membrane electroporation in an imbalanced ion distribution. These are typical cases in which the SPICA FF using the non-polar water model fails to show high performance. In addition to surface and elastic properties comparable to those of the experiment, CG-MDs performed with pSPICA can provide more realistic electrostatic interactions necessary to capture membrane water defects and pores, which are important for many biological processes.[22,23]

In this study, to overcome the limitations arising from the use of non-polar CG water to simulate lipid-protein systems, we developed a CG protein model that is fully compatible with the lipid and water models in the pSPICA FF. Protein interaction parameters were adjusted to reproduce several thermodynamic quantities and structural data from both the experiments and AA-MD simulations, following the optimization protocol used in the SPICA FF. CG-MD simulations with the obtained parameter sets yields results that were in good agreement with the reference data. In addition, several CG-MDs were performed in application studies to validate the model. CG-MDs of melittin peptides forming transmembrane pores were conducted to compare the stability of the pores using polar and non-polar water models. The mechanosensitive channel of large conductance (MscL), a homopentamer

channel, was used to assess whether the stability and structure of the protein assembly were comparable to those of AA-MDs. Furthermore, the adsorption of nona-arginine (R9) peptides on lipid membranes at different salt concentrations was simulated. These application studies demonstrate the importance of electrostatic screening effects, which were properly accounted for by employing a polar CG water model. The pSPICA FF parameters are freely available from the SPICA website (https://www.spica-ff.org). The protein parameters were employed in our previous work on the antimicrobial actions of melittin (version 1.0).[24] The parameters were further optimized in this work and distributed as version 1.1.

The remainder of this paper is organized as follows. In Section 2, we describe the details of pSPICA, that is, the potential functions, the introduced protein model, and the simulation methods used in this study. Section 3 presents the results of CG parameterization and application studies of lipid-protein systems. The conclusions of this study are presented in Section 4.

2 Methods

2.1 Coarse-grained model

This subsection outlines the protein CG model of pSPICA.[21] The CG modeling scheme of pSPICA basically follows that of SPICA. The definitions of the CG units of the proteins in pSPICA was the same as those used in SPICA. The backbone (BB) atoms of one amino acid are represented by a single CG unit (GBB or ABB) placed on the α-carbon atom. The SC atoms are mapped to 0–4 CG units placed at the center of mass of the heavy atoms in each CG unit, as shown in Figure S1. The protein models established in this study are fully compatible with the pSPICA lipid and water models. The pSPICA water model represents three water molecules as two charged CG units linked by a rigid bond. The LJ interaction was considered only for the negatively charged CG unit of the water model. The standard

Coulomb potential function was used to describe electrostatic interactions:

$$U_{\mathrm{coul}}(r_{ij}) = \frac{q_i q_j}{4\pi\varepsilon_0\varepsilon_{\mathrm{r}} r_{ij}}, \tag{1}$$

where q_i is the partial charge of ith particle, ε_0 is the permittivity in vacuum, and ε_{r} is the relative dielectric constant. A value of $\varepsilon_{\mathrm{r}} = 3.2$ is applied in pSPICA to reproduce experimental values of bulk water properties, such as the density, surface tension, and electrostatic permittivity. For the LJ interaction, the following three function types (LJ12-5, LJ12-4, and LJ9-6) were used separately:

$$U_{\mathrm{LJ}}(r_{ij}) = \begin{cases} \dfrac{12}{7}\left(\dfrac{12}{5}\right)^{\left(\frac{5}{7}\right)}\varepsilon_{ij}\left[\left(\dfrac{\sigma_{ij}}{r_{ij}}\right)^{12} - \left(\dfrac{\sigma_{ij}}{r_{ij}}\right)^{5}\right] \\ \dfrac{3\sqrt{3}}{2}\varepsilon_{ij}\left[\left(\dfrac{\sigma_{ij}}{r_{ij}}\right)^{12} - \left(\dfrac{\sigma_{ij}}{r_{ij}}\right)^{4}\right] \\ \dfrac{27}{4}\varepsilon_{ij}\left[\left(\dfrac{\sigma_{ij}}{r_{ij}}\right)^{9} - \left(\dfrac{\sigma_{ij}}{r_{ij}}\right)^{6}\right], \end{cases} \tag{2}$$

where ε_{ij} and σ_{ij} are the minimum energy and distance at which U_{LJ} equals zero because the prefactors of all LJ functions are determined to satisfy $U_{\mathrm{LJ}}(\sigma_{ij}) = 0$ and $\min\{U_{\mathrm{LJ}}(r_{ij})\} = -\varepsilon_{ij}$. The LJ12-5 function was applied to the pairs of water and ions. The interaction for pairs between the uncharged CG units and water were described using the LJ12-4 function. The LJ9-6 function was applied to pairs other than those described above. All the LJ interactions are truncated at a distance of $r_{\mathrm{cut}} = 15$ Å. For bonded interactions, the bond stretching and angle bending are expressed by the following harmonic potentials:

$$U_{\mathrm{bond}}(r) = k_{\mathrm{bond}}(r - r_0)^2, \tag{3}$$

$$U_{\mathrm{angle}}(\theta) = k_{\mathrm{angle}}(\theta - \theta_0)^2, \tag{4}$$

where k_{bond} and k_{angle} are the force constants, and r_0 and θ_0 are the equilibrium length and angle, respectively. The following bonded interaction for the dihedral angle was also employed to maintain the cyclic SCs (phenylalanine and tyrosine) in the plane:

$$U_{\mathrm{dihedral}}(\phi) = k_{\mathrm{dihedral}}[1 + \cos(\phi - d)], \tag{5}$$

where k_{dihedral} and d are the force constant and phase of the dihedral angles, respectively. To preserve the secondary structure of the proteins in the CG simulations, an elastic network model (ENM) described by harmonic potentials was employed. Elastic network bonds were generated between protein BB units within a distance of 9 Å. The force constant of the harmonic potential for the elastic network was selected as 1.195 kcal/Å^2/mol.

The bonded parameters for the CG proteins in pSPICA were the same as those in SPICA. For nonbonded interaction parameters between uncharged SCs, we employed the same parameters as those determined in a previous study for SPICA protein modeling.[17,25] Other LJ interactions were optimized by carrying out a series of CG simulations of proteins in this work, as described later.

2.2 Simulation setup

The CG protein structures used in the simulations were prepared by mapping crystal structures obtained from the PDB databank (https://www.rcsb.org). We used the CHARMM-GUI membrane builder[26] to generate configurations of fully hydrated lipid membranes and mapped them to a CG representation. The mapping from AA to CG was performed using a set of Python codes distributed at https://github.com/SPICA-group/spica-tools.

All CG simulations for the parameterization were conducted using LAMMPS software.[27] The bond length in the CG water was maintained at a constant length using the SHAKE algorithm.[28] Electrostatic interactions were calculated using the PPPM method.[29] LJ interactions were truncated at 15 Å. Energy minimization of the simulated systems was performed

using the conjugate gradient method. The MD time step was set to 10 fs, to ensure energy conservation in the NVE simulations using pSPICA. The system pressure was maintained at 1 atm using a Parrinello-Rahman barostat,[30] and the system temperature was maintained at 310 K (physiological temperature) using a Nosé-Hoover thermostat.[31,32] However, depending on the reference data, we slightly changed the system temperature in the simulations to 298, 303, and 308 K, as shown below. Strictly speaking, CG models are not temperature-transferable because the lost entropy within the CG unit cannot be compensated in the same way for different temperatures. As seen in a previous study, pSPICA showed good temperature transferability from 290 to 363 K for water.[21] Lipid membrane properties such as area per lipid and thickness from CG-MDs with pSPICA were verified to be in good agreement with experimental data at 298 to 323 K.[21] Thus, the minor temperature change in the parameterization of the pSPICA protein model should have a negligible impact on the resultant parameters.

AA-MD simulations were conducted with the CHARMM36 FF[33,34] and TIP3P water model[35] using GROMACS software[36] to generate the reference data for the parameterization of the CG model. Energy minimization was performed using the steepest descent method. The pressure and temperature of the system were set to the same conditions as those calculated for the CG systems and maintained with a Parrinello-Rahman barostat[30] and a Nosé-Hoover thermostat.[31,32] Electrostatic interactions were calculated using the Particle Mesh Ewald (PME) method.[37] LJ interactions were truncated at 12 Å with a smooth switching function in a range of 10−12 Å. The geometric structure of the water molecules was kept constant using the SETTLE algorithm.[38] The LINCS algorithm[39] was applied to constrain all bonds involving hydrogen atoms (except for water molecules) and to use a time-step size of 2 fs. The parameters of simulated SC analogues and their dimers, namely non-protein molecules, were assigned based on the protein parameters of the CHARMM36 FF (for the details, see Supporting Information), and all configuration, topology, and parameter files required for AA simulations of both SC analogue monomers and dimers can be

found at our repository presented in Data Availability section.

Errors of simulation results were calculated as the standard deviation from three replica runs, unless otherwise noted. Simulation visualization and plotting were performed using Visual Molecular Dynamics (VMD) software[40] and Matplotlib,[41] respectively. Additional software used for analyses were Colvars module[42] and MDAnalysis.[43,44]

3 Results and discussion

3.1 Parameter optimization

As mentioned above, we used the same LJ parameters for the pairs of uncharged SCs as in the previous study,[45] because the parameters had been already optimized for the experimental density and surface tension of SC analogue liquid (not dependent on water models). In this section, the other nonbonded parameters were determined according to the scheme shown in Table 1. The optimization was conducted manually and systematically. The compound names corresponding to the SC analogues are listed in Table S1.

Table 1: Order of optimization, target properties, and adjusted parameters in CG parameterization

Order	target properties	adjusted pair
I	interfacial tension at SC analogue/water interface	SC[a]–water
II	hydration free energy of SC analogue	SC[b]–water
III	density of SC analogue solution	SC[c]–water
IV	radial distribution function of SC analogue dimers in water	SC[c]–SC
V	free energy profile of SC analogue across the lipid membrane	SC–lipid
VI	penetration depths and tilt angles of peripheral peptides/proteins	BB–lipid/water
VII	dimerization free energy of transmembrane helices	BB–BB/SC

[a] uncharged hydrophobic
[b] uncharged hydrophilic
[c] charged

3.1.1 Protein side chain parameters

First, we simulated SC analogue systems for parameter fitting with reference to the experimental interfacial tension at the SC analogue/water interface, the experimental hydration free energy of SC analogues, or the solution density and radial distribution functions (RDFs) of SC analogues obtained from AA-MDs. In SPICA protein modeling, the parameters between uncharged SC analogues and water were determined with reference to the hydration free energy data. However, this model was found to underestimate the interfacial tension between the hydrophobic SC analogue and water compared to the experimental data. In keeping with the original SPICA philosophy of accurately reproducing interfacial properties, the reproduction of the interfacial tension at the SC analogue/water interface was prioritized over the reproduction of the hydration free energy of the SC analogue. As pointed out in SPICA protein modeling, reproducing the hydration free energy of a charged SC analogue would overestimate its interaction with water. Using these parameters, water particles coordinated to charged SC analogues would freeze, resulting in problems in sampling hydrated protein structures. Instead, the interactions involved in the charged SC analogues were adjusted by referring to the solution density and RDFs.

The SC analogue/water interfacial tensions were calculated to tune the LJ parameters for hydrophobic SCs, namely, valine, leucine, isoleucine, and phenylalanine, against water. Except phenylalanine, we used dimers composed of two SC analogues covalently linked to each other to calculate the interfacial tensions, because the monomers of the SC analogues exhibit a gas phase at the target temperature. We constructed two-component systems consisting of approximately 350 hydrophobic SCs and 650 water particles. After confirming the formation of the SC analogue (dimer)/water interface in the systems, we further performed simulations as equilibration and production MD runs at 303 K in an NP_zAT ensemble. The production run lasted 20 ns, and the last 10 ns were used to estimate the interfacial tension using a pressure tensor. The calculated interfacial tension values are listed in Table 2. For the VAL dimer system, an experimental value obtained from the hexane/water system is

shown. The values calculated using pSPICA were consistent with the experimental data. Although the experimental values of the interfacial tension for the LEU and ILE dimer systems were not available, the calculated values captured the trend that the longer the alkane chain, the greater the interfacial tension.[46]

The hydration free energies of the SCs were calculated to optimize the LJ parameters between the uncharged hydrophilic SC analogues and water. We calculated the work required to pull a single side chain from bulk water (1000 particles) to a vacuum perpendicular to the vacuum-water interface in the NVT ensemble. The force constant and pulling velocity were set as 1 kcal/Å/mol and 1 Å/ns, respectively. We estimated the free energy difference by calculating the ten-times exponential average of the work using the Jarzynski equality.[47] The system temperature was set to 298 K, as in the experiment. The obtained hydration free energies of each SC are listed in Table 3 along with the experimental data. The difference in the free energy between the CG model and experimental data was at most 0.18 kcal/mol for TYR, and the agreement between the simulated and experimental hydration free energy values was very good for all hydrophilic SC analogues.

The LJ interactions between charged SC analogues were adjusted to reproduce the reference data obtained from AA-MD simulations, including the RDFs of the two SC analogue dimers and the density of the SC analogue dimer solution. The simulated systems consisted of 24 SC analogue dimers, approximately 650 water particles, and counter ions. RDFs were also used to fix the parameters between the charged and uncharged SCs. The system temperature and pressure were set at 310 K and 1 atm, respectively. We performed 10 ns MD simulations for each system in the NPT ensemble, and the last 5 ns were used to calculate the RDFs and density. Table 4 lists the obtained densities of the charged SC solutions, which were in good agreement with the experimental values. Moreover, all the calculated RDFs are shown in Figure S2, indicating that they reproduced the AA results well. To verify that the LJ parameters between the uncharged SCs, determined based on the Lorentz-Berthelot combination rule, worked effectively in pSPICA, we calculated the potential mean force (PMF)

between the SC analogues in aqueous solution, as plotted in Figure S3. The difference of the first minimum between the CG and AA PMF was less than 1 kcal/mol. Thus, all LJ interactions between the SC analogues and water were well-optimized with reference to the AA-MD simulations and experimental data.

Table 2: SC analogue (dimer)/water interfacial tension (mN/m) at 303 K[45,48]

SC	pSPICA	Exp
ILE	52.3±0.4	···
LEU	51.3±0.3	···
VAL(PRO)	50.0±0.3	50.0
PHE	36.2±0.3	36.0

Table 3: Hydration free energy of SC analogues (kcal/mol) at 298 K[49,50]

SC	pSPICA	Exp
HIS	-10.21 ± 0.25	-10.25
ASN	-9.81 ± 0.03	-9.68
GLN	-9.38 ± 0.08	-9.38
TRP	-5.77 ± 0.20	-5.88
SER	-5.20 ± 0.13	-5.06
THR	-4.93 ± 0.04	-4.88
TYR	-3.03 ± 0.07	-3.17
MET	-1.68 ± 0.09	-1.48
CYS	-1.23 ± 0.02	-1.24

Table 4: Density (kg/m^3) of charged SC analogue dimer solution at 310 K

SC	pSPICA	CHARMM36
ASP	1089.2±0.5	1084.9±0.2
GLU	1085.9±0.1	1080.2±0.1
ARG	1040.7±0.1	1038.3±0.1
LYS	1021.0±0.1	1020.7±0.1

To tune the LJ parameters between the SC analogues and lipids, we calculated the transfer free energy of the SC analogues from water to the lipid bilayer center. Free energy was

calculated along the z-distance between the SC analogue and the membrane center. The target systems at atomic resolution consisted of 72 palmitoyloleoylphosphatydylcholine (POPC) lipids and approximately 3750 water particles, and were neutralized with sodium or chloride ions as needed. The systems for the CG model were almost identical to those obtained by the CG mapping of the AA configuration. To calculate the free energy using the adaptive biasing force (ABF) method,[51,52] the AA simulations were conducted using NAMD 2.11.[53] The system temperature and pressure were controlled at 310 K and 1 atm, respectively, using a Langevin thermostat and a barostat,[54] respectively. Six windows spanning from 0 to 30 Å with a width of 5 Å were prepared, and 100 ns MD sampling was performed for each window in the $NP_{xy}P_zT$ ensemble. The free energy calculation setup for AA-MD simulations was almost the same as that for CG-MD simulations. Because the convergence of free energy calculations in AA-MD simulations is slower than that in CG-MD simulations, AA-MD simulations were performed for 200 ns as a production run for each window. The calculated free energy profiles of the charged SCs across the POPC bilayer are shown in Figure 1. The AA- and CG-MD results were in good agreement for all SC analogues. Similarly, almost identical AA and CG free energy profiles were found for uncharged SC analogues, as shown in Figure S4. It is important to note, the barrier height of the free energy for charged SC analogues at the membrane center was well reproduced with the present pSPICA model, though this was significantly underestimated by SPICA FF.[17] The extra energy cost found in pSPICA arose from the deformation of the membrane owing to the formation of water string (defect) with charged SC analogues when inserted into the membrane center. Figure 2 shows the water defects produced by the insertion of arginine into the membrane core. A similar water defect was not observed by CG-MD with SPICA using non-polar CG water.[17,55,56] As will be shown later, the stability of the water string is directly related to the structural stability of the narrow channel formed by proteins or peptides across the bilayer membranes.

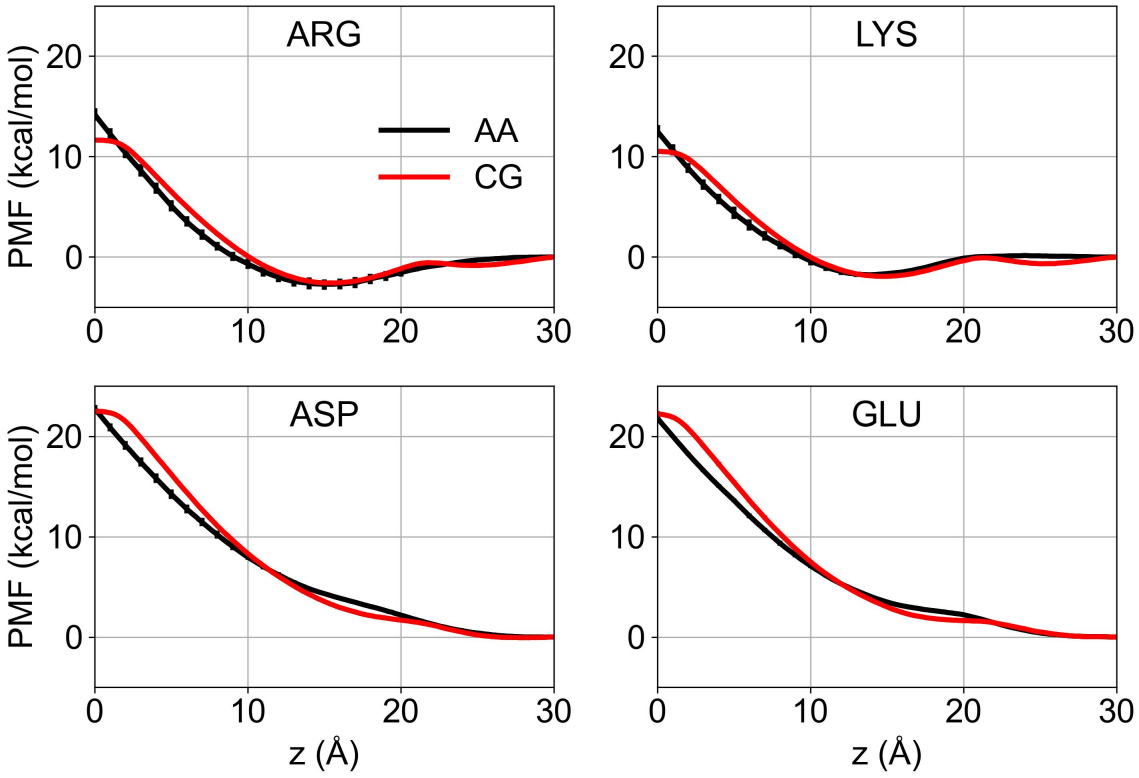

Figure 1: Transfer free energy profiles of charged SC analogues along the POPC bilayer normal, obtained from CG-MD using pSPICA FF and AA-MD using CHARMM36 FF. The error bars given represent standard errors, which can be smaller than line thickness of the plots.

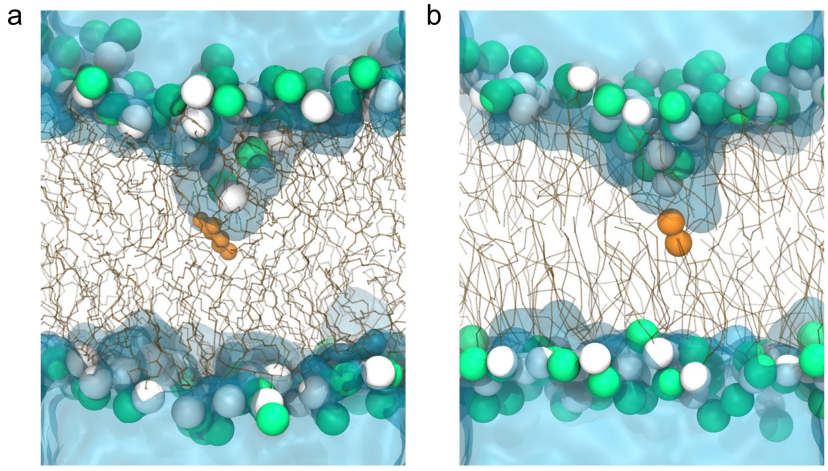

Figure 2: Snapshots of a water defect on a POPC membrane owing to the insertion of an arginine analogue, as modeled using (a) CHARMM36 and (b) pSPICA. The arginine analogue is shown in orange. Lipid headgroups and tail particles are represented as VDW spheres and licorice, respectively. Water is represented as transparent cyan.

3.1.2 Protein backbone parameters

The LJ parameters between the BB units and water/lipids were adjusted to reproduce the penetration depth and tilt angle of the peripheral peptides obtained from the OPM database.[57] The reference data for 96 peripheral α-helical peptides extracted from the OPM database were used for parameter optimization. In the initial configuration, each peptide was placed approximately 20 Å away from a membrane consisting of 128 dioleoylphosphatidylcholine (DOPC) molecules. Approximately 3400–4800 CG water particles were used to hydrate the peptides and membranes in the system, and sodium or chloride ions were added to maintain charge neutrality. To efficiently sample peptides interacting with lipid membranes, it was necessary to avoid diffusion of the peptides from the membrane into the aqueous solution. Thus, a wall potential was placed at a distance of 25 Å from the membrane surface and applied only to the centers of mass of the peptides and lipid membrane to accelerate their contact. The CG-MD simulation was run for 300 ns, and the last 100 ns of the MD trajectories were used for analysis. The results obtained for the anchoring depth and tilt angle of α-helical peptides are shown in Figure S5. For almost all the calculated peptides,

the penetration depth and tilt angle simulated using pSPICA FF were in good agreement with those of the OPM data.

We optimized the LJ parameters between the BB units and between BB units and SC analogues with reference to the dimerization free energy of the transmembrane peptides. As in a previous study,[17] five types of the transmembrane peptides were used: WALP,[58] GpA,[59,60] SerZipper,[61] EphA1,[62] and ErbB1.[63] The details of the simulated system are provided in Table S2. The dimerization free energies were calculated by PMF along the cylindrical distance between the centers of mass of the two peptides using the ABF method. ABF sampling was performed for 500 ns in each of six windows of 5 Å width in a range of 3 to 33 Å. The calculated dimerization free energies are shown in Table 5. The obtained PMFs are shown in Figure S6. The dimerization free energies estimated by CG-MD with pSPICA FF captured the experimental data well, although the free energy of the EphA1 dimer slightly underestimated the experimental value.

Thus, we followed the modeling scheme of the SPICA protein and successfully generated all necessary pSPICA parameters for the CG-MD of lipid-protein systems.

Table 5: Dimerization free energies of transmembrane peptides (kcal/mol)

Peptide dimer	pSPICA	Exp
WALP	-3.2 ± 0.4	-2.2–-6.2[58]
GpA	-5.2 ± 0.1	-3.2–-7.5[59,60]
SerZip	-7.1 ± 1.2	< -8[61]
EphA1	-2.1 ± 0.2	-3.7 ± 0.1[62]
ErbB1	-2.6 ± 0.5	-2.5 ± 0.1[63]

3.2 Applications

3.2.1 Antimicrobial peptides

Many MD simulations have been performed to investigate the interaction of antimicrobial peptides (AMPs) with the lipid membrane and the mechanism of pore formation.[24,64–76]

However, the stability of membrane pores induced by AMPs is strongly dependent on the water models used in the CG-MD simulation,[56] and the membrane water defect is an important event to be captured for pore simulations, especially when using CG models. In our previous study, we successfully observed membrane pore formation induced by melittin, a representative AMP, and focused on the pore formation process and its mechanism depending on the protein-lipid ratio.[24] Here, we performed CG simulations to assess the stability of the membrane pore formed by melittins. The initial configuration was generated by mapping the AA configuration, obtained from the AA-MD in our study,[76] to the CG configuration, which consisted of 128 POPC lipids, six melittins, CG water, and counter ions. For comparison, the CG-MD simulations of three replicas with different initial velocity were performed using the pSPICA FF and SPICA FF. Figure 3a and 3b show the final snapshots after 1 μs CG-MD using pSPICA and SPICA, respectively. Figure 3c and 3d show the time variation of the number of CG water particles present in the pore formed by melittins simulated with pSPICA and SPICA, respectively. In the simulations with pSPICA, the pore formed by the melittins remained open, along with the water channel across the membrane. In contrast, in the simulations with SPICA, the water channel across the membrane was completely closed, though the melittins remained bridging across the membrane until the end of the simulations. The results indicate that the stability of the water channel is quite different between the nonpolar and polar water models, even though they were built using the same parameterization scheme. The radius of the pore in the CG-MD with pSPICA was estimated by calculating the number density of the lipid tails along the lateral distance from the pore center (Figure S7). The MD trajectory was analyzed from 0 to 0.4 μs, where all the melittins contributed to maintaining the pore. The radial distance at which the number density first reached half of the maximum was measured, as in the previous study.[76] The estimated average radius for the three runs was approximately 18 Å and similar to the previous AA-MD value of 22 Å,[76] supporting that pSPICA can accurately predict the membrane pore structure formed by AMPs.

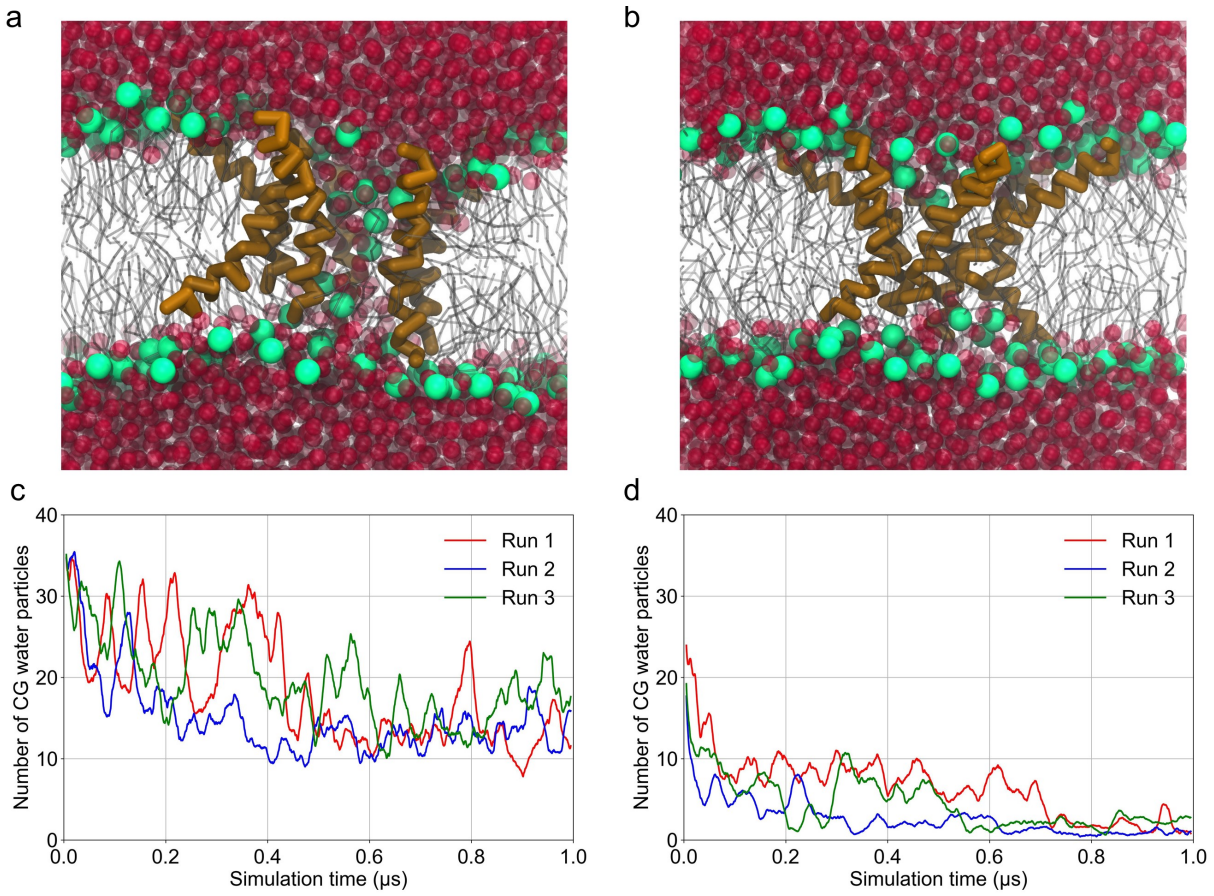

Figure 3: Snapshots of the final configuration of CG simulations using (a) pSPICA and (b) SPICA. Melittin peptides, phosphate groups, and lipid tails are represented by brown licorice, green VDW sphere, and gray transparent lines, respectively. CG water particles are shown in a transparent red VDW representation. (c) and (d) show time evolution of the number of CG water particles in the membrane pore maintained by melittin peptides in CG simulations using pSPICA and SPICA, respectively. Each line shows 200 ns rolling average for each different run.

3.2.2 Mechanosensitive channel of large conductance

MscL are the assemblies of multiple transmembrane peptides that regulate ion permeation in response to membrane tension. The detailed structure of MscL in *Mycobacterium tuberculosis* was experimentally obtained,[77] and based on the structure, gating of MscL has been extensively studied using MD simulations.[78–82] To compare the stability and structure of MscL simulated using pSPICA to AA simulation results[82] for validation, we performed CG simulations of MscL (PDBID:2OAR) embedded in a DOPC membrane consisting of 365 lipids. The membrane was hydrated by 12003 CG water, and ions were added to realize 150 mM NaCl solution. The cytoplasmic region beyond Ala110 of the MscL residues was excised in this simulation because it was suggested to be unimportant for MscL gating.[78,80] The system pressure in the simulation of MscL in the closed state was controlled at a hydrostatic pressure of 1 atm. For the simulation of MscL in the open state, we applied a surface tension of 75 mN/m according to the previous study,[82] although the value appears to be larger than experiments using patch-clamps.[83] CG simulations with and without surface tension at 310 K were carried out for 1 μs each. The calculated root-mean-square deviation (RMSD) of the MscL backbone with respect to the initial structure over time showed an increasing trend for the three replicated MD runs under applied tension (Figure S8a), but not for the three replicated MD runs without tension (Figure S8b). This indicates that in CG simulations using pSPICA, the MscL embedded in the lipid bilayer responds appropriately to the applied tension and shows a transition from the closed to the open state. Although only one of three replica runs provided the fully open structure of MscL within the 1 μs simulation (Figure S8a: Run 1), the MscLs in the other two replica runs also show a structural change to the open state, and it is probably only a matter of time before they open completely. The final snapshots of the closed and the open states are shown in Figure 4a and Figure 4b, respectively. Figure 4c shows the radii of MscLs along the z-distance from the membrane center calculated using the HOLE program.[84] MD trajectories of 0.7 – 1.0 μs were used to calculate the radius, as it took about 0.7 μs to reach the channel open state under membrane

tension condition (Figure S8a: Run 1). The narrowest channel radius of 1.6 Å calculated from CG-MD with pSPICA was within the radius range of 1.0–1.8 Å estimated from AA-MD,[82] although a lipid membrane composed of saturated lipids was used in the AA-MD. These results indicate that MscL maintains the channel structure and responds reasonably well to the applied surface tension in CG-MD with pSPICA, which is consistent with the AA-MD results. We also performed CG-MD on the same system using SPICA to compare ion transport across the membrane with that using pSPICA. The number of sodium and chloride ions that passed through the membrane during the simulations are listed in Table 6. Under surface tension, some ions could translocate across the membrane in the simulations with both pSPICA and SPICA. MscL in the closed state simulated with pSPICA completely blocked ion translocation, whereas CG-MD with SPICA allowed the translocation of some ions across the membrane but not through MscL. The transfer free energy of CG ions (i.e., ions hydrated by a few water molecules) across the membrane was significantly underestimated owing to the assumption of a large relative permittivity in SPICA FF.[15] pSPICA can thus provide a reasonable description of ion transport through MscL, which is consistent with the AA-MD and experimental results.[85,86] Note that the pore radius in the open state of MscL is sufficient to allow the membrane transport of CG water, sodium ions, and chloride ions in pSPICA.

Table 6: The number of CG sodium and chloride ions permeated through MscL during 1μs CG simulations

Model	State	Sodium	Chloride
pSPICA	open	9	14
	closed	0	0
SPICA	open	30	9
	closed	7	8

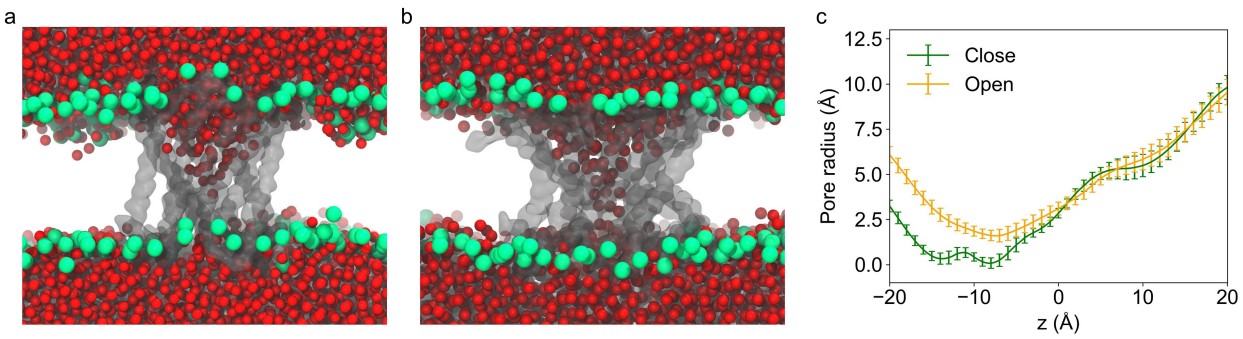

Figure 4: Snapshots of MscLs embedded in DOPC lipid membranes. (a) closed and (b) open states simulated with pSPICA. MscL is shown in transparent gray. Water and lipid phosphate particles are represented by red and green particles, respectively. (c) Radius profiles of MscL pores along the z-distance from the membrane center. The error bars are given by standard deviation over simulation time.

3.2.3 Adsorption of nona-arginine onto lipid membranes

The present CG protein model was designed to target peripheral and transmembrane peptides; reproducing protein adsorption on lipid membrane surfaces was not the main target. However, to evaluate the performance of pSPICA in peptide adsorption, we chose R9, which has been studied by AA-MD,[87] as a model peptide and investigated how membrane adsorption is modified by salt concentration using CG-MD. Bilayer systems (consisting of 200 POPC lipids and 12 R9 peptides) with different salt concentrations were prepared for CG-MD. These membrane systems were hydrated with approximately 4600 CG water: one system was simply neutralized by adding counter ions (chloride), and the other system was adjusted to a 560 mM NaCl solution by adding more salt. CG-MD runs (1 μs) of three replicas started with different velocity assignment for both systems were performed using pSPICA. The final snapshots of the CG-MD runs in salt-free and 560 mM NaCl solution are shown in Figure 5a and Figure 5b, respectively. The R9 peptides formed aggregates in CG-MD, and the size of the aggregates in the 560 mM NaCl solution appeared to be larger than that in the salt-free solution. Electrostatic repulsion among the R9 peptides suppressed the aggregation of the peptides in the salt-free solution. In contrast, the electrostatic re-

pulsion weakened by the screening effect of the salt promoted aggregation in the 560 mM NaCl solution. These results are consistent with those of the AA-MD and experimental studies.[88] Figure 5c and 5d show the time evolution of the minimum distance between each R9 and the membrane in the salt-free and 560 mM NaCl solutions, respectively. The minimum distance is about 5 Å, corresponding to R9 bound to the membrane surface. All R9 peptides in the salt-free system were adsorbed to the membrane surface immediately after starting CG-MD, whereas some R9 peptides in the 560 mM NaCl solution showed reversible membrane adsorption. The strong binding of R9 to the membrane surface and the propensity for membrane-binding behavior depending on salt concentration were similar to those observed in AA simulations.[87,89,90] The reversible membrane binding might be caused by the competition for the interaction of R9 peptides with their aggregates and the membrane. These observations confirmed that pSPICA is useful for simulating protein adsorption on the membrane surface.

4 Conclusions

We extended the pSPICA FF to allow CG-MD simulations of biological systems including proteins, using a polar water CG model. The interactions between uncharged SCs and water were tuned by fitting the experimental solvation free energy of SC analogues and SC analogue/water interfacial tension. For charged SC analogues, the calculated density of the SC analogue dimer solution and the RDFs between SC analogue dimers obtained from the AA-MDs were used to adapt the interaction. The transfer free energy profiles of SC analogues across the lipid membrane calculated using the developed model showed excellent agreement with those calculated using the CHARMM36 FF. The high free energy barriers around the membrane hydrophobic core in the PMF profiles for the charged SCs obtained from CG-MDs were comparable to those obtained from AA-MDs, reflecting properly sustained water string formation due to the inserted charged SCs in the CG-MDs. The interactions related to the

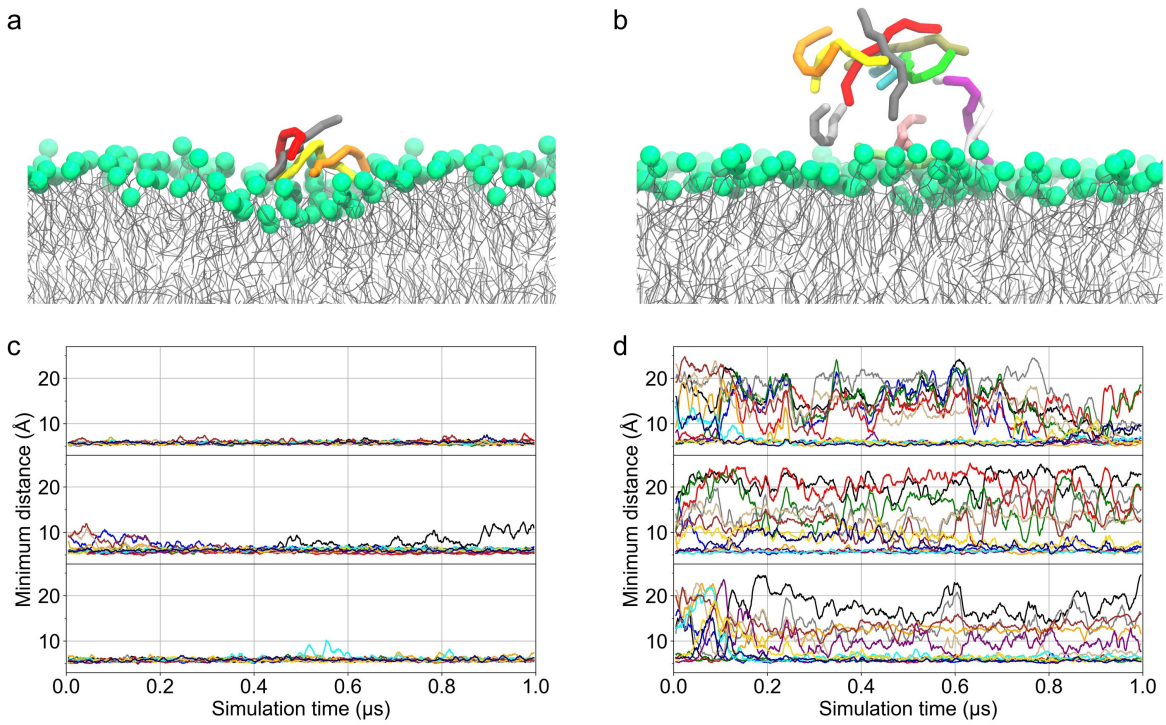

Figure 5: Snapshots of R9 peptides adsorbed on a POPC lipid membrane in (a) salt-free and (b) 560 mM NaCl solution. Minimum distance between each R9 peptide and a POPC lipid membrane during CG simulations at (c) salt-free and (d) 560 mM NaCl concentrations for three different runs. Each peptide is indicated by a different color.

BB units were optimized to reproduce the penetration depth and tilt angles of the peptides on the lipid membrane, taken from the OPM database, and the dimerization free energy of five types of transmembrane proteins. We then tested the developed model by performing CG simulations on several lipid-protein systems. The membrane pore structure maintained by multiple melittin peptides simulated with pSPICA was in good agreement with the result observed in our previous AA-MD study.[76] The MscL embedded in the lipid membrane was stable in the simulation, and the radius of the MscL pore in the open state was in good agreement with that calculated for AA-MD.[82] In addition, ion transport across the membrane through MscL was reasonable. The effect of salt concentration on the adsorption of cationic R9 peptides on lipid membrane surfaces was adequately reproduced and was consistent with the experimental and AA-MD observations.[87,89,90] Although we thus successfully observed the reasonable adsorption of the R9 peptides in our simulation, we may need to consider the secondary-structure dependent BB parameters, as introduced in an improved SPICA protein model,[19] to address more generally the protein adsorption on the lipid membrane. The developed CG protein model could correctly simulate molecular processes, especially those involving transmembrane pores, and overcome the accuracy limitations of using uncharged CG water models.

Data Availability

Topologies, initial coordinates, input files, and analysis codes for our MD simulations are openly available at https://doi.org/10.5281/zenodo.10224805.

Supporting Information

The Supporting Information is available free of charge at http://pubs.acs.org/doi/***.

CG mapping of each amino acids in the pSPICA FF. Chemical nomenclature of SC analogues. Comparison of AA and CG-MD results for radial distribution functions and potential

mean forces between SC dimers in aqueous solution. Transfer free energy profiles for uncharged SCs across a POPC membrane. Penetration depths and tilt angles of peripheral peptides on DOPC membrane. Free energy profile between transmembrane helices in lipid membranes and the detailed information of the simulated systems. Density of lipid tail group along lateral radial distance from the center of membrane pore generated by melittin peptides. Time evolution of root-mean-square deviation of MscL. Preparation of SC analogues for AA simulations. (PDF)

Acknowledgments

This study was supported by JSPS KAKENHI (grant number JP 21H01880). This research used the computational facilities of Research Center for Computational Science, Okazaki, Japan (Project:22-IMS-C108, 23-IMS-C095) and the Institute for Solid State Physics, the University of Tokyo, Japan.

References

(1) Enkavi, G.; Javanainen, M.; Kulig, W.; Róg, T.; Vattulainen, I. Multiscale simulations of biological membranes: The challenge to understand biological phenomena in a living substance. *Chem. Rev.* **2019**, *119*, 5607–5774.

(2) Noid, W. G. Perspective: Advances, challenges, and insight for predictive coarse-grained models. *J. Phys. Chem. B* **2023**, *127*, 4174–4207.

(3) Shih, A. Y.; Arkhipov, A.; Freddolino, P. L.; Schulten, K. Coarse grained protein-lipid model with application to lipoprotein particles. *J. Phys. Chem. B* **2006**, *110*, 3674–3684.

(4) Marrink, S. J.; Risselada, H. J.; Yefimov, S.; Tieleman, D. P.; De Vries, A. H. The

MARTINI force field: Coarse grained model for biomolecular simulations. *J. Phys. Chem. B* **2007**, *111*, 7812–7824.

(5) Wan, C.-K.; Han, W.; Wu, Y.-D. Parameterization of PACE force field for membrane environment and simulation of helical peptides and helix-helix association. *J. Chem. Theory Comput.* **2012**, *8*, 300–313.

(6) Darré, L.; Machado, M. R.; Brandner, A. F.; González, H. C.; Ferreira, S.; Pantano, S. SIRAH: A structurally unbiased coarse-grained force field for proteins with aqueous solvation and long-range electrostatics. *J. Chem. Theory Comput.* **2015**, *11*, 723–739.

(7) Zięba, K.; Ślusarz, M.; Ślusarz, R.; Liwo, A.; Czaplewski, C.; Sieradzan, A. K. Extension of the UNRES coarse-grained force field to membrane proteins in the lipid bilayer. *J. Phys. Chem. B* **2019**, *123*, 7829–7839.

(8) Ugarte La Torre, D.; Takada, S. Modeling lipid–protein interactions for coarse-grained lipid and Cα protein models. *J. Chem. Phys.* **2021**, *155*, 155101.

(9) Yu, A.; Pak, A. J.; He, P.; Monje-Galvan, V.; Casalino, L.; Gaieb, Z.; Dommer, A. C.; Amaro, R. E.; Voth, G. A. A multiscale coarse-grained model of the SARS-CoV-2 virion. *Biophys. J.* **2021**, *120*, 1097–1104.

(10) Souza, P. C. T.; Alessandri, R.; Barnoud, J.; Thallmair, S.; Faustino, I.; Grünewald, F.; Patmanidis, I.; Abdizadeh, H.; Bruininks, B. M. H.; Wassenaar, T. A.; Kroon, P. C.; Melcr, J.; Nieto, V.; Corradi, V.; Khan, H. M.; Domański, J.; Javanainen, M.; Martinez-Seara, H.; Reuter, N.; Best, R. B.; Vattulainen, I.; Monticelli, L.; Periole, X.; Tieleman, D. P.; de Vries, A. H.; Marrink, S. J. Martini 3: A general purpose force field for coarse-grained molecular dynamics. *Nat. Methods* **2021**, *18*, 382–388.

(11) Seo, S.; Shinoda, W. SPICA force field for lipid membranes: Domain formation induced by cholesterol. *J. Chem. Theory Comput.* **2019**, *15*, 762–774.

(12) Shinoda, W.; Devane, R.; Klein, M. L. Multi-property fitting and parameterization of a coarse grained model for aqueous surfactants. *Mol. Simul.* **2007**, *33*, 27–36.

(13) Shinoda, W.; DeVane, R.; Klein, M. L. Coarse-grained molecular modeling of non-ionic surfactant self-assembly. *Soft Matter* **2008**, *4*, 2454–2462.

(14) Shinoda, W.; Devane, R.; Klein, M. L. Zwitterionic lipid assemblies: Molecular dynamics studies of monolayers, bilayers, and vesicles using a new coarse grain force field. *J. Phys. Chem. B* **2010**, *114*, 6836–6849.

(15) Shinoda, W.; DeVane, R.; Klein, M. L. Coarse-grained force field for ionic surfactants. *Soft Matter* **2011**, *7*, 6178–6186.

(16) Shinoda, W.; DeVane, R.; Klein, M. L. Computer simulation studies of self-assembling macromolecules. *Curr. Opin. Struct. Biol.* **2012**, *22*, 175–186.

(17) Kawamoto, S.; Liu, H.; Miyazaki, Y.; Seo, S.; Dixit, M.; Devane, R.; MacDermaid, C.; Fiorin, G.; Klein, M. L.; Shinoda, W. SPICA force field for proteins and peptides. *J. Chem. Theory Comput.* **2022**, *18*, 3204–3217.

(18) Zoni, V.; Khaddaj, R.; Lukmantara, I.; Shinoda, W.; Yang, H.; Schneiter, R.; Vanni, S. Seipin accumulates and traps diacylglycerols and triglycerides in its ring-like structure. *Proc. Natl. Acad. Sci. U. S. A.* **2021**, *118*, e2017205118.

(19) Yamada, T.; Miyazaki, Y.; Harada, S.; Kumar, A.; Vanni, S.; Shinoda, W. Improved protein model in SPICA force field. *J. Chem. Theory Comput.* in press, DOI: 10.1021/acs.jctc.3c01016.

(20) Klauda, J. B.; Venable, R. M.; Freites, J. A.; O'Connor, J. W.; Tobias, D. J.; Mondragon-Ramirez, C.; Vorobyov, I.; MacKerell, A. D.; Pastor, R. W. Update of the CHARMM all-atom additive force field for lipids: Validation on six lipid types. *J. Phys. Chem. B* **2010**, *114*, 7830–7843.

(21) Miyazaki, Y.; Okazaki, S.; Shinoda, W. pSPICA: A coarse-grained force field for lipid membranes based on a polar water model. *J. Chem. Theory Comput.* **2020**, *16*, 782–793.

(22) Bennett, W. F. D.; Spacy, N.; Tieleman, D. P. Atomistic simulations of pore formation and closure in lipid bilayers. *Biophys. J.* **2014**, *106*, 210–219.

(23) Bennett, W. F. D.; Tieleman, D. P. The importance of membrane defects—lessons from simulations. *Acc. Chem. Res.* **2014**, *47*, 2244–2251.

(24) Miyazaki, Y.; Shinoda, W. Cooperative antimicrobial action of melittin on lipid membranes: A coarse-grained molecular dynamics study. *Biochim. Biophys. Acta, Biomembr.* **2022**, *1864*, 183955.

(25) Devane, R.; Shinoda, W.; Moore, P. B.; Klein, M. L. Transferable coarse grain non-bonded interaction model for amino acids. *J. Chem. Theory Comput.* **2009**, *5*, 2115–2124.

(26) Wu, E. L.; Cheng, X.; Jo, S.; Rui, H.; Song, K. C.; Dávila-Contreras, E. M.; Qi, Y.; Lee, J.; Monje-Galvan, V.; Venable, R. M.; Klauda, J. B.; Im, W. CHARMM-GUI membrane builder toward realistic biological membrane simulations. *J. Comput. Chem.* **2014**, *35*, 1997–2004.

(27) Thompson, A. P.; Aktulga, H. M.; Berger, R.; Bolintineanu, D. S.; Brown, W. M.; Crozier, P. S.; in 't Veld, P. J.; Kohlmeyer, A.; Moore, S. G.; Nguyen, T. D.; Shan, R.; Stevens, M. J.; Tranchida, J.; Trott, C.; Plimpton, S. J. LAMMPS - a flexible simulation tool for particle-based materials modeling at the atomic, meso, and continuum scales. *Comput. Phys. Commun.* **2022**, *271*, 108171.

(28) Ryckaert, J. P.; Ciccotti, G.; Berendsen, H. J. Numerical integration of the cartesian equations of motion of a system with constraints: molecular dynamics of n-alkanes. *J. Comput. Phys.* **1977**, *23*, 327–341.

(29) Hockney, R. W.; Eastwood, J. W. *Computer Simulation Using Particles*; CRC Press, 1988.

(30) Parrinello, M.; Rahman, A. Polymorphic transitions in single crystals : A new molecular dynamics method. *J. Appl. Phys.* **1981**, *52*, 7182–7190.

(31) Nosé, S. A unified formulation of the constant temperature molecular dynamics methods. *J. Chem. Phys.* **1984**, *81*, 511–519.

(32) Hoover, W. G. Canonical dynamics: Equilibrium phase-space distributions. *Phys. Rev. A* **1985**, *31*, 1695–1697.

(33) Klauda, J. B.; Venable, R. M.; Freites, J. A.; O'Connor, J. W.; Tobias, D. J.; Mondragon-Ramirez, C.; Vorobyov, I.; MacKerell, A. D.; Pastor, R. W.; Pastor, R. W. Update of the CHARMM all-atom additive force field for lipids: Validation on six lipid types. *The J. Phys. Chem. B* **2010**, *114*, 7830–43.

(34) Best, R. B.; Zhu, X.; Shim, J.; Lopes, P. E.; Mittal, J.; Feig, M.; MacKerell, A. D. Optimization of the additive CHARMM all-atom protein force field targeting improved sampling of the backbone ϕ, ψ and side-chain $\chi1$ and $\chi2$ dihedral angles. *J. Chem. Theory Comput.* **2012**, *8*, 3257–3273.

(35) Jorgensen, W. L.; Chandrasekhar, J.; Madura, J. D.; Impey, R. W.; Klein, M. L. Comparison of simple potential functions for simulating liquid water. *J. Chem. Phys.* **1983**, *79*, 926–935.

(36) Abraham, M. J.; Murtola, T.; Schulz, R.; Páll, S.; Smith, J. C. GROMACS: High performance molecular simulations through multi-level parallelism from laptops to supercomputers. *SoftwareX* **2015**, *1-2*, 19–25.

(37) Darden, T.; York, D.; Pedersen, L. Particle mesh Ewald - An N·log(N) method for Ewald sums in large systems. *J. Chem. Phys.* **1993**, *98*, 10089–10092.

(38) Miyamoto, S.; Kollman, P. A. Settle: An analytical version of the SHAKE and RATTLE algorithm for rigid water models. *J. Comput. Chem.* **1992**, *13*, 952–962.

(39) Hess, B.; Bekker, H.; Berendsen, H. J. C. LINCS: A linear constraint solver for molecular simulations. *J. Comput. Chem.* **1997**, *18*, 1463–1472.

(40) Humphrey, W.; Dalke, A.; Schulten, K. VDM: visual molecular dynamics. *J. Mol. Graph.* **1996**, *14*, 33–38.

(41) Hunter, J. D. Matplotlib: A 2D graphics environment. *Comput. Sci. Eng.* **2007**, *9*, 90–95.

(42) Fiorin, G.; Hénin, J.; Chipot, C.; Klein, M. L. Using collective variables to drive molecular dynamics simulations. *Mol. Phys.* **2013**, *111*, 3345–3362.

(43) Gowers, R. J.; Linke, M.; Barnoud, J.; Reddy, T. J. E.; Melo, M. N.; Seyler, S. L.; Domański, J.; Dotson, D. L.; Buchoux, S.; Kenney, I. M.; Beckstein, O. MDAnalysis: A Python Package for the Rapid Analysis of Molecular Dynamics Simulations. Proceedings of the 15th Python in Science Conference. 2016; pp 98–105.

(44) Michaud-Agrawal, N.; Denning, E. J.; Woolf, T. B.; Beckstein, O. MDAnalysis: A toolkit for the analysis of molecular dynamics simulations. *J. Comput. Chem.* **2011**, *32*, 2319–2327.

(45) Devane, R.; Klein, M. L.; Chiu, C. C.; Nielsen, S. O.; Shinoda, W.; Moore, P. B. Coarse-grained potential models for phenyl-based molecules: I. Parametrization using experimental data. *J. Phys. Chem. B* **2010**, *114*, 6386–6393.

(46) Goebel, A.; Lunkenheimer, K. Interfacial tension of the water/n-alkane interface. *Langmuir* **1997**, *13*, 369–372.

(47) Park, S.; Schulten, K. Calculating potentials of mean force from steered molecular dynamics simulations. *J. Chem. Phys.* **2004**, *120*, 926–1420.

(48) CRC Handbook, *CRC Handbook of Chemistry and Physics, 88th Edition*, 88th ed.; CRC Press, 2007.

(49) Sharp, K. A.; Nicholls, A.; Friedman, R.; Honig, B. Extracting hydrophobic free energies from experimental data: Relationship to protein folding and theoretical models. *Biochemistry* **1991**, *30*, 9686–9697.

(50) Shirts, M. R.; Pande, V. S. Solvation free energies of amino acid side chain analogs for common molecular mechanics water models. *J. Chem. Phys.* **2005**, *122*, 134508.

(51) Darve, E.; Rodríguez-Gómez, D.; Pohorille, A. Adaptive biasing force method for scalar and vector free energy calculations. *J. Chem. Phys.* **2008**, *128*, 144120.

(52) Hénin, J.; Fiorin, G.; Klein, M. L. Exploring multidimensional free energy landscapes using time-dependent biases on collective variables. *J. Chem. Theory Comput.* **2010**, *6*, 35–47.

(53) Phillips, J. C.; Braun, R.; Wang, W.; Gumbart, J.; Tajkhorshid, E.; Villa, E.; Chipot, C.; Skeel, R. D.; Kalé, L.; Schulten, K. Scalable molecular dynamics with NAMD. *J. Comput. Chem.* **2005**, *26*, 1781–1802.

(54) Feller, S. E.; Zhang, Y.; Pastor, R. W.; Brooks, B. R. Constant pressure molecular dynamics simulation: The Langevin piston method. *J. Chem. Phys.* **1995**, *103*, 4613–4621.

(55) Monticelli, L.; Kandasamy, S. K.; Periole, X.; Larson, R. G.; Tieleman, D. P.; Marrink, S. J. The MARTINI coarse-grained force field: Extension to proteins. *J. Chem. Theory Comput.* **2008**, *4*, 819–834.

(56) Bennett, W. F.; Tieleman, D. P. Water defect and pore formation in atomistic and coarse-grained lipid membranes: Pushing the limits of coarse graining. *J. Chem. Theory Comput.* **2011**, *7*, 2981–2988.

(57) Lomize, M. A.; Lomize, A. L.; Pogozheva, I. D.; Mosberg, H. I. OPM: Orientations of proteins in membranes database. *Bioinformatics* **2006**, *22*, 623–625.

(58) Yano, Y.; Matsuzaki, K. Measurement of thermodynamic parameters for hydrophobic mismatch 1: Self-association of a transmembrane helix. *Biochemistry* **2006**, *45*, 3370–3378.

(59) Chen, L.; Novicky, L.; Merzlyakov, M.; Hristov, T.; Hristova, K. Measuring the energetics of membrane protein dimerization in mammalian membranes. *J. Am. Chem. Soc.* **2010**, *132*, 3628–3635.

(60) Sarabipour, S.; Hristova, K. Glycophorin A transmembrane domain dimerization in plasma membrane vesicles derived from CHO, HEK 293T, and A431 cells. *Biochim. Biophys. Acta, Biomembr.* **2013**, *1828*, 1829–1833.

(61) North, B.; Cristian, L.; Stowell, X. F.; Lear, J. D.; Saven, J. G.; DeGrado, W. F. Characterization of a membrane protein folding motif, the Ser zipper, using designed peptides. *J. Mol. Biol.* **2006**, *359*, 930–939.

(62) Artemenko, E. O.; Egorova, N. S.; Arseniev, A. S.; Feofanov, A. V. Transmembrane domain of EphA1 receptor forms dimers in membrane-like environment. *Biochim. Biophys. Acta, Biomembr.* **2008**, *1778*, 2361–2367.

(63) Chen, L.; Merzlyakov, M.; Cohen, T.; Shai, Y.; Hristova, K. Energetics of ErbB1 transmembrane domain dimerization in lipid bilayers. *Biophys. J.* **2009**, *96*, 4622–4630.

(64) Sengupta, D.; Leontiadou, H.; Mark, A. E.; Marrink, S. J. Toroidal pores formed by antimicrobial peptides show significant disorder. *Biochim. Biophys. Acta* **2008**, *1778*, 2308–2317.

(65) Manna, M.; Mukhopadhyay, C. Cause and effect of melittin-induced pore formation: A computational approach. *Langmuir* **2009**, *25*, 12235–12242.

(66) Santo, K. P.; Berkowitz, M. L. Difference between magainin-2 and melittin assemblies in phosphatidylcholine bilayers: Results from coarse-grained simulations. *J. Phys. Chem. B* **2012**, *116*, 3021–3030.

(67) Santo, K. P.; Irudayam, S. J.; Berkowitz, M. L. Melittin creates transient pores in a lipid bilayer: Results from computer simulations. *J. Phys. Chem. B* **2013**, *117*, 5031–5042.

(68) Chen, C. H.; Wiedman, G.; Khan, A.; Ulmschneider, M. B. Absorption and folding of melittin onto lipid bilayer membranes via unbiased atomic detail microsecond molecular dynamics simulation. *Biochim. Biophys. Acta* **2014**, *1838*, 2243–2249.

(69) Sun, D.; Forsman, J.; Woodward, C. E. Amphipathic membrane-active peptides recognize and stabilize ruptured membrane pores: Exploring cause and effect with coarse-grained simulations. *Langmuir* **2015**, *31*, 752–761.

(70) Sun, D.; Forsman, J.; Woodward, C. E. Multistep molecular dynamics simulations identify the highly cooperative activity of melittin in recognizing and stabilizing membrane pores. *Langmuir* **2015**, *31*, 9388–9401.

(71) Upadhyay, S. K.; Wang, Y.; Zhao, T.; Ulmschneider, J. P. Insights from micro-second atomistic simulations of melittin in thin lipid bilayers. *J. Membr. Biol.* **2015**, *248*, 497–503.

(72) Sun, D.; Forsman, J.; Woodward, E. Molecular simulations of melittin-induced membrane pores. *J. Phys. Chem. B* **2017**, *121*, 10209–10214.

(73) Lyu, Y.; Xiang, N.; Zhu, X.; Narsimhan, G. Potential of mean force for insertion of antimicrobial peptide melittin into a pore in mixed DOPC/DOPG lipid bilayer by molecular dynamics simulation. *J. Chem. Phys.* **2017**, *146*, 155101.

(74) Pino-angeles, A.; Lazaridis, T. Effects of peptide charge, orientation, and concentration on melittin transmembrane pores. *Biophys. J.* **2018**, *114*, 2865–2874.

(75) Shi, Y.; Wan, M.; Fu, L.; Zhang, S.; Wang, S.; Gao, L.; Fang, W. Peptide-lipid interaction sites affect vesicles' responses to antimicrobial peptides. *Biophys. J.* **2018**, *115*, 1518–1529.

(76) Miyazaki, Y.; Okazaki, S.; Shinoda, W. Free energy analysis of membrane pore formation process in the presence of multiple melittin peptides. *Biochim. Biophys. Acta, Biomembr.* **2019**, *1861*, 1409–1419.

(77) Steinbacher, S.; Bass, R.; Strop, P.; Rees, D. C. Structures of the prokaryotic mechanosensitive channels MscL and MscS. *Curr. Top. Membr.* **2007**, *58*, 1–24.

(78) Colombo, G.; Marrink, S. J.; Mark, A. E. Simulation of MscL gating in a bilayer under stress. *Biophys. J.* **2003**, *84*, 2331–2337.

(79) Gullingsrud, J.; Schulten, K. Gating of MscL studied by steered molecular dynamics. *Biophys. J.* **2003**, *85*, 2087–2099.

(80) Sawada, Y.; Sokabe, M. Molecular dynamics study on protein–water interplay in the mechanogating of the bacterial mechanosensitive channel MscL. *Eur. Biophys. J.* **2015**, *44*, 531–543.

(81) Melo, M. N.; Arnarez, C.; Sikkema, H.; Kumar, N.; Walko, M.; Berendsen, H. J. C.; Kocer, A.; Marrink, S. J.; Ingólfsson, H. I. High-throughput simulations reveal membrane-mediated effects of alcohols on MscL gating. *J. Am. Chem. Soc.* **2017**, *139*, 2664–2671.

(82) Katsuta, H.; Sawada, Y.; Sokabe, M. Biophysical mechanisms of membrane-thickness-dependent MscL gating: An all-atom molecular dynamics study. *Langmuir* **2019**, *35*, 7432–7442.

(83) Sukharev, S. I.; Sigurdson, W. J.; Kung, C.; Sachs, F. Energetic and spatial parameters for gating of the bacterial large conductance mechanosensitive channel, MscL . *J. Gen. Physiol.* **1999**, *113*, 525–540.

(84) Smart, O. S.; Neduvelil, J. G.; Wang, X.; Wallace, B.; Sansom, M. S. HOLE: A program for the analysis of the pore dimensions of ion channel structural models. *J. Mol. Graph.* **1996**, *14*, 354–360.

(85) Mukherjee, N.; Jose, M. D.; Birkner, J. P.; Walko, M.; Ingólfsson, H. I.; Dimitrova, A.; Arnarez, C.; Marrink, S. J.; Koçer, A. The activation mode of the mechanosensitive ion channel, MscL, by lysophosphatidylcholine differs from tension-induced gating. *The FASEB Journal* **2014**, *28*, 4292–4302.

(86) Naeini, V. F.; Baniassadi, M.; Foroutan, M.; Rémond, Y.; George, D. Decisive structural elements in water and ion permeation through mechanosensitive channels of large conductance: insights from molecular dynamics simulation. *RSC Adv.* **2022**, *12*, 17803–17816.

(87) Nguyen, M. T. H.; Biriukov, D.; Tempra, C.; Baxova, K.; Martinez-Seara, H.; Evci, H.; Singh, V.; Šachl, R.; Hof, M.; Jungwirth, P.; Javanainen, M.; Vazdar, M. Ionic strength and solution composition dictate the adsorption of cell-penetrating peptides onto phosphatidylcholine membranes. *Langmuir* **2022**, *38*, 11284–11295.

(88) Tesei, G.; Vazdar, M.; Jensen, M. R.; Cragnell, C.; Mason, P. E.; Heyda, J.; Skepö, M.; Jungwirth, P.; Lund, M. Self-association of a highly charged arginine-rich cell-penetrating peptide. *Proc. Natl. Acad. Sci. U. S. A.* **2017**, *114*, 11428–11433.

(89) Vazdar, M.; Wernersson, E.; Khabiri, M.; Cwiklik, L.; Jurkiewicz, P.; Hof, M.; Mann, E.; Kolusheva, S.; Jelinek, R.; Jungwirth, P. Aggregation of oligoarginines at phospholipid membranes: Molecular dynamics simulations, time-dependent fluorescence shift, and biomimetic colorimetric assays. *J. Phys. Chem. B* **2013**, *117*, 11530–11540.

(90) Sun, D.; Forsman, J.; Woodward, C. E. Atomistic molecular simulations suggest a kinetic model for membrane translocation by arginine-rich peptides. *J. Phys. Chem. B* **2015**, *119*, 14413–14420.

TOC Graphic